

The Higgs boson decay $h \rightarrow bs$ in the $U(1)_X$ SSM

Song Gao^{1,2,3}, Shu-Min Zhao^{1,2,3*}, Ming-Yue Liu^{1,2,3},

Xing-Yu Han^{1,2,3}, Xi Wang^{1,2,3}, Tai-Fu Feng^{1,2,3,4},

¹ *Department of Physics, Hebei University, Baoding 071002, China*

² *Hebei Key Laboratory of High-precision Computation and Application of Quantum Field Theory, Baoding, 071002, China*

³ *Hebei Research Center of the Basic Discipline for Computational Physics, Baoding, 071002, China and*

⁴ *Department of Physics, Chongqing University, Chongqing 401331, China*

(Dated: May 28, 2024)

Abstract

In the $U(1)_X$ SSM, we delve into the flavor violation of $h \rightarrow bs$, where h is identified with the SM-like Higgs boson discovered at the LHC. As the $U(1)$ extension of the minimal supersymmetric standard model (MSSM), the $U(1)_X$ SSM has new super fields such as right-handed neutrinos and three Higgs singlets. We conduct a thorough analysis of the underlying mechanisms and parameter dependencies of $h \rightarrow bs$ in the $U(1)_X$ SSM. In the $U(1)_X$ SSM, we discover that the $\text{Br}(h \rightarrow bs)$ for the Higgs decay to bs could significantly differ from the expectation in the standard model (SM), depending on the values of the new parameters introduced in the model. Our research not only contributes to a deeper understanding of Higgs physics within the $U(1)_X$ SSM, but also provides valuable guidance for new physics (NP).

PACS numbers:

Keywords: $U(1)_X$ SSM, Higgs boson, new physics

* zhaosm@mail.nankai.edu.cn; 17713155332@163.com

I. INTRODUCTION

After the discovery of the Higgs boson[1–7], one of the main goals has been to measure its properties with the highest possible precision. Current measurements, within experimental and theoretical uncertainties, are consistent with the predictions of the SM for the Higgs boson. Flavor-changing Higgs interactions provide an intriguing scenario for searching for new physics. In the SM, flavor-changing neutral currents (FCNC) occur only at the loop level and are thus highly suppressed[8]. Therefore, physics beyond the SM may predict larger FCNC compared to the SM. The initial studies of the loop-induced hbs coupling originate in the 1980s[9], while more recent work based on current data reports that the predicted $h \rightarrow bs$ in the SM is approximately 10^{-7} [10–13].

Subsequently, scientists broaden the scope of the SM and derived numerous extended models, with the MSSM garnering significant attention. However, it has gradually become apparent that the MSSM faces issues, including the neutrinos mass and mixing[14, 15], μ problem[16, 17] and the Higgs mass problem[18]. To address these challenges, we have turned our attention to the $U(1)$ extension of the MSSM. Specifically, $U(1)_X$ SSM is an extended model based on MSSM, and the local gauge group is $SU(3)_C \times SU(2)_L \times U(1)_Y \times U(1)_X$ [19–22]. Comparing with MSSM, $U(1)_X$ SSM has more superfields including: right handed neutrinos and three Higgs singlets[23, 24]. By studying the decay modes of the Higgs boson, particularly FCNC decays, which may enhance $\text{Br}(h \rightarrow bs)$ in the $U(1)_X$ SSM, we can gain a deeper understanding of the coupling strengths and nature of the Higgs boson interactions with quarks. It can elucidate the physical essence of the Higgs boson.

Some researchers study the decay of $h \rightarrow bs$ under the Two Higgs Doublet Model (2HDM)[8, 25]. Their research mainly analyzed the impact of the $\lambda_{hH^+H^-}$ parameter and Yukawa types in 2HDM on the $h \rightarrow bs$ decay. $\lambda_{hH^+H^-}$ may lead to significant deviations from the SM predictions, but it still satisfies the current constraints of 2HDM. Finally, they concluded that the $Br^{2HDM}(h \rightarrow bs)$ is of the order of 10^{-3} , which is of great assistance to our subsequent research on the $h \rightarrow bs$ decay in the $U(1)_X$ SSM.

The outline of this paper is as follows, in Sec.II, we will introduce the fundamental elements of the $U(1)_X$ SSM, including its superpotential, general soft-breaking terms, the mass-squared matrix of the CP-even Higgs at the tree level, as well as the mass matrices and coupling vertices we will utilize. In Sec.III, we will provide analytical expressions for

the branching ratio of the $h \rightarrow bs$ decay in the $U(1)_X$ SSM. In Sec.IV, we present the corresponding parameters and numerical analysis. In Sec.V, we offer a summary of this article. Some formulas are shown in the appendix.

II. THE RELEVANT CONTENT OF $U(1)_X$ SSM

The local gauge group of $U(1)_X$ SSM contains the four components $SU(3)_C \times SU(2)_L \times U(1)_Y \times U(1)_X$. As an extension of MSSM, it adds three new Higgs singlets, $\hat{\eta}$, $\hat{\bar{\eta}}$, \hat{S} and also introduces three generations of right-handed neutrinos labelled $\hat{\nu}_i$. Compared with MSSM, $U(1)_X$ SSM exhibits notable advantages, which are as follows

1. By introducing additional free parameters, the $U(1)_X$ SSM can more naturally satisfy the experimental data from the LHC.
2. Through the seesaw mechanism, the light neutrinos acquire tiny masses at the tree level.
3. The neutral CP-even parts of the introduced $\hat{\eta}$, $\hat{\bar{\eta}}$, \hat{S} , H_u and H_d and mix together, forming a 5×5 mass-squared matrix. Consequently, the mass of the lightest CP-even Higgs particle can be improved at the tree level[27].

The superpotential of $U(1)_X$ SSM is expressed as follows

$$W = l_W S + \mu H_u H_d + M_S S S - Y_d \hat{d} \hat{q} H_d - Y_e \hat{e} \hat{l} H_d + \lambda_H S H_u H_d + \lambda_C S \eta \bar{\eta} + \frac{\kappa}{3} S S S + Y_u \hat{u} \hat{q} H_u + Y_X \hat{\nu} \bar{\eta} \hat{\nu} + Y_\nu \hat{\nu} \hat{l} H_u. \quad (1)$$

We use the notations of v_u , v_d , v_η , $v_{\bar{\eta}}$ and v_S to signify the vacuum expectation values (VEVs) associated with the Higgs superfields H_u , H_d , v_η , $v_{\bar{\eta}}$, and S , respectively. Subsequently, we present the precise formulations of the two Higgs doublets and three Higgs singlets here

$$H_u = \begin{pmatrix} H_u^+ \\ \frac{1}{\sqrt{2}}(v_u + H_u^0 + iP_u^0) \end{pmatrix}, H_d = \begin{pmatrix} \frac{1}{\sqrt{2}}(v_d + H_d^0 + iP_d^0) \\ H_d^- \end{pmatrix}, \\ \eta = \frac{1}{\sqrt{2}}(v_\eta + \phi_\eta^0 + iP_\eta^0), \quad \bar{\eta} = \frac{1}{\sqrt{2}}(v_{\bar{\eta}} + \phi_{\bar{\eta}}^0 + iP_{\bar{\eta}}^0), \quad S = \frac{1}{\sqrt{2}}(v_S + \phi_S^0 + iP_S^0). \quad (2)$$

And two angles are defined as $\tan \beta = v_u/v_d$ and $\tan \beta_\eta = v_{\bar{\eta}}/v_\eta$.

The soft SUSY breaking terms of $U(1)_X$ SSM are as follows

$$\mathcal{L}_{soft} = \mathcal{L}_{soft}^{MSSM} - B_S S^2 - L_S S - \frac{T_\kappa}{3} S^3 - T_{\lambda_C} S \eta \bar{\eta} + \epsilon_{ij} T_{\lambda_H} S H_d^i H_u^j$$

TABLE I: The superfields in $U(1)_X$ SSM

Superfields	\hat{q}_i	\hat{u}_i^c	\hat{d}_i^c	\hat{l}_i	\hat{e}_i^c	$\hat{\nu}_i$	\hat{H}_u	\hat{H}_d	$\hat{\eta}$	$\hat{\bar{\eta}}$	\hat{S}
$SU(3)_C$	3	$\bar{3}$	$\bar{3}$	1	1	1	1	1	1	1	1
$SU(2)_L$	2	1	1	2	1	1	2	2	1	1	1
$U(1)_Y$	1/6	-2/3	1/3	-1/2	1	0	1/2	-1/2	0	0	0
$U(1)_X$	0	-1/2	1/2	0	1/2	-1/2	1/2	-1/2	-1	1	0

$$\begin{aligned}
 & -T_X^{IJ} \bar{\eta} \tilde{\nu}_R^{*I} \tilde{\nu}_R^{*J} + \epsilon_{ij} T_\nu^{IJ} H_u^i \tilde{\nu}_R^{I*} \tilde{l}_j^J - m_\eta^2 |\eta|^2 - m_{\bar{\eta}}^2 |\bar{\eta}|^2 - m_S^2 S^2 \\
 & - (m_{\tilde{\nu}_R}^2)^{IJ} \tilde{\nu}_R^{I*} \tilde{\nu}_R^J - \frac{1}{2} \left(M_S \lambda_{\hat{X}}^2 + 2M_{BB'} \lambda_{\hat{B}} \lambda_{\hat{X}} \right) + h.c.
 \end{aligned} \tag{3}$$

$\mathcal{L}_{soft}^{MSSM}$ represents the soft breaking terms of MSSM.

In the context of $U(1)_X$ SSM, the simultaneous existence of two Abelian groups, $U(1)_Y$ and $U(1)_X$, gives rise to a new effect that does not exist in MSSM: gauge kinetic mixing. This effect can also be induced through Renormalization Group Equations (RGEs) even with zero at M_{GUT} .

Y^Y denotes the $U(1)_Y$ charge, while Y^X represents the $U(1)_X$ charge. One can write the covariant derivatives of the $U(1)_X$ SSM in the following form[28–30]

$$D_\mu = \partial_\mu - i \left(Y^Y, Y^X \right) \begin{pmatrix} g_Y & g'_{YX} \\ g'_{XY} & g'_X \end{pmatrix} \begin{pmatrix} A'_\mu{}^Y \\ A'_\mu{}^X \end{pmatrix}, \tag{4}$$

where $A'_\mu{}^Y$ and $A'_\mu{}^X$ represent the gauge fields of $U(1)_Y$ and $U(1)_X$, respectively.

Under the condition that the two Abelian gauge groups remain unbroken, we employ the rotation matrix R to carry out a change of basis[30]

$$\begin{pmatrix} g_Y & g'_{YX} \\ g'_{XY} & g'_X \end{pmatrix} R^T = \begin{pmatrix} g_1 & g_{YX} \\ 0 & g_X \end{pmatrix}, \quad R \begin{pmatrix} A'_\mu{}^Y \\ A'_\mu{}^X \end{pmatrix} = \begin{pmatrix} A_\mu^Y \\ A_\mu^X \end{pmatrix}, \tag{5}$$

In the end, the covariant derivatives of the $U(1)_X$ SSM transform into

$$D_\mu = \partial_\mu - i \left(Y^Y, Y^X \right) \begin{pmatrix} g_1 & g_{YX} \\ 0 & g_X \end{pmatrix} \begin{pmatrix} A_\mu^Y \\ A_\mu^X \end{pmatrix}. \tag{6}$$

At the tree level, three neutral gauge bosons A_μ^X , A_μ^Y , and $V_\mu'^3$ mix with each other, with

their mass matrix represented in the basis of (A'_μ, V'^3, A'^X) .

$$\begin{pmatrix} \frac{1}{8}g_1^2v^2, & -\frac{1}{8}g_1g_2v^2, & \frac{1}{8}g_1(g_{YX} + g_X)v^2 \\ -\frac{1}{8}g_1g_2v^2, & \frac{1}{8}g_1g_2v^2, & -\frac{1}{8}g_2(g_X + g_{YX})v^2 \\ (g_{YX} + g_X)v^2, & (g_{YX} + g_X)v^2, & \frac{1}{8}g_X^2\xi^2 \end{pmatrix}, \quad (7)$$

with $v^2 = v_u^2 + v_d^2$ and $\xi^2 = v_\eta^2 + v_{\bar{\eta}}^2$.

At the tree level, the mass-squared matrix for the CP-even Higgs $(\phi_d, \phi_u, \phi_\eta, \bar{\phi}_\eta, \phi_s)$ is as follows

$$M_h^2 = \begin{pmatrix} m_{\phi_d\phi_d} & m_{\phi_u\phi_d} & m_{\phi_\eta\phi_d} & m_{\phi_{\bar{\eta}}\phi_d} & m_{\phi_s\phi_d} \\ m_{\phi_d\phi_u} & m_{\phi_u\phi_u} & m_{\phi_\eta\phi_u} & m_{\phi_{\bar{\eta}}\phi_u} & m_{\phi_s\phi_u} \\ m_{\phi_d\phi_\eta} & m_{\phi_u\phi_\eta} & m_{\phi_\eta\phi_\eta} & m_{\phi_{\bar{\eta}}\phi_\eta} & m_{\phi_s\phi_\eta} \\ m_{\phi_d\phi_{\bar{\eta}}} & m_{\phi_u\phi_{\bar{\eta}}} & m_{\phi_\eta\phi_{\bar{\eta}}} & m_{\phi_{\bar{\eta}}\phi_{\bar{\eta}}} & m_{\phi_s\phi_{\bar{\eta}}} \\ m_{\phi_d\phi_s} & m_{\phi_u\phi_s} & m_{\phi_\eta\phi_s} & m_{\phi_{\bar{\eta}}\phi_s} & m_{\phi_s\phi_s} \end{pmatrix}, \quad (8)$$

$$m_{\phi_d\phi_d} = m_{H_d}^2 + \mu^2 + \frac{1}{8} \left([g_1^2 + (g_X + g_{YX})^2 + g_2^2] (3v_d^2 - v_u^2) + 2(g_{YX}g_X + g_X^2)(v_\eta^2 - v_{\bar{\eta}}^2) \right) + \sqrt{2}v_S\mu\lambda_H + \frac{1}{2}(v_u^2 + v_S^2)\lambda_H^2, \quad (9)$$

$$m_{\phi_d\phi_u} = -\frac{1}{4} \left(g_2^2 + (g_{YX} + g_X)^2 + g_1^2 \right) v_d v_u + \lambda_H^2 v_d v_u - \lambda_H l_W - \frac{1}{2} \lambda_H v_\eta v_{\bar{\eta}} \lambda_C + v_S^2 \kappa - B_\mu - \sqrt{2}v_S \left(\frac{1}{2} T_{\lambda_H} + M_S \lambda_H \right), \quad (10)$$

$$m_{\phi_u\phi_u} = m_{H_u}^2 + \mu^2 + \frac{1}{8} \left\{ \left([g_1^2 + (g_X + g_{YX})^2 + g_2^2] \right) (3v_u^2 - v_d^2) + 2(g_{YX}g_X + g_X^2)(v_\eta^2 - v_{\bar{\eta}}^2) \right\} + \sqrt{2}v_S\mu\lambda_H + \frac{1}{2}(v_d^2 + v_S^2)\lambda_H^2, \quad (11)$$

$$m_{\phi_d\phi_\eta} = \frac{1}{2}g_X(g_{YX} + g_X)v_d v_\eta - \frac{1}{2}v_u v_{\bar{\eta}} \lambda_H \lambda_C, \quad (12)$$

$$m_{\phi_u\phi_\eta} = -\frac{1}{2}g_X(g_{YX} + g_X)v_d v_\eta - \frac{1}{2}v_d v_{\bar{\eta}} \lambda_H \lambda_C, \quad (13)$$

$$m_{\phi_\eta\phi_\eta} = m_\eta^2 + \frac{1}{4} \left([(g_{YX}g_X + g_X^2)](v_d^2 - v_u^2) + 2g_X^2(3v_\eta^2 - v_{\bar{\eta}}^2) \right) + \frac{\lambda_C^2}{2}(v_\eta^2 + v_S^2), \quad (14)$$

$$m_{\phi_d\phi_{\bar{\eta}}} = -\frac{1}{2}g_X(g_{YX} + g_X)v_d v_\eta - \frac{1}{2}v_u v_{\bar{\eta}} \lambda_H \lambda_C, \quad (15)$$

$$m_{\phi_u\phi_{\bar{\eta}}} = \frac{1}{2}g_X(g_{YX} + g_X)v_d v_\eta - \frac{1}{2}v_d v_{\bar{\eta}} \lambda_H \lambda_C, \quad (16)$$

$$m_{\phi_\eta\phi_{\bar{\eta}}} = (\lambda_C^2 - g_X^2)v_\eta v_{\bar{\eta}} + \frac{\lambda_C}{2}(2l_W - \lambda_H v_d v_u) + \frac{v_S}{\sqrt{2}}(2M_S \lambda_C + T_{\lambda_C}) + \frac{v_S^2}{2} \lambda_C \kappa, \quad (17)$$

$$m_{\phi_{\bar{\eta}}\phi_{\bar{\eta}}} = m_{\bar{\eta}}^2 + \frac{1}{4} \left((g_{YX}g_X + g_X^2)(v_u^2 - v_d^2) + 2g_X^2(3v_{\bar{\eta}}^2 - v_\eta^2) \right) + \frac{\lambda_C^2}{2}(v_\eta^2 + v_S^2), \quad (18)$$

$$m_{\phi_d\phi_s} = \left(\lambda_H v_d v_S + \sqrt{2} v_d \mu - v_u (\kappa v_S + \sqrt{2} M_S) \right) \lambda_H - \frac{1}{\sqrt{2}} v_u T_{\lambda_H}, \quad (19)$$

$$m_{\phi_u\phi_s} = \left(\lambda_H v_u v_S + \sqrt{2} v_u \mu - v_d (\kappa v_S + \sqrt{2} M_S) \right) \lambda_H - \frac{1}{\sqrt{2}} v_d T_{\lambda_H}, \quad (20)$$

$$m_{\phi_\eta\phi_s} = \left(\lambda_C v_\eta v_S + v_{\bar{\eta}} (\kappa v_S + \sqrt{2} M_S) \right) \lambda_C + \frac{1}{\sqrt{2}} v_{\bar{\eta}} T_{\lambda_C}, \quad (21)$$

$$m_{\phi_{\bar{\eta}}\phi_s} = \left(\lambda_C v_{\bar{\eta}} v_S + v_\eta (\kappa v_S + \sqrt{2} M_S) \right) \lambda_C + \frac{1}{\sqrt{2}} v_\eta T_{\lambda_C}, \quad (22)$$

$$m_{\phi_s\phi_s} = m_S^2 + \left(2l_W + 3v_S (\kappa v_S + 2\sqrt{2} M_S) + \lambda_C v_\eta v_{\bar{\eta}} - \lambda_H v_d v_u \right) \kappa + 2B_S \\ + \frac{1}{2} \lambda_C^2 \xi^2 + \frac{1}{2} \lambda_H^2 v^2 + 4M_S^2 + \sqrt{2} v_S T_\kappa. \quad (23)$$

This matrix is diagonalized by Z^H

$$Z^H M_h^2 Z^{H,\dagger} = M_{2,h}^{dia}. \quad (24)$$

The mass matrix for charginos in the basis: $(\tilde{W}^-, \tilde{H}_d^-), (\tilde{W}^+, \tilde{H}_u^+)$

$$M_{\tilde{\chi}^\pm} = \begin{pmatrix} M_2 & \frac{1}{\sqrt{2}} g_2 v_u \\ \frac{1}{\sqrt{2}} g_2 v_d & \frac{1}{\sqrt{2}} \lambda_H v_S + \mu \end{pmatrix}, \quad (25)$$

The matrix is diagonalized by U and V

$$U^* M_{\tilde{\chi}^\pm} V^\dagger = M_{\tilde{\chi}^\pm}^{dia}. \quad (26)$$

Moreover, down type scalar quark squared mass matrix M_D^2 , up type scalar quark squared mass matrix M_U^2 and neutralino mass matrix $M_{\tilde{\chi}^0}$ are needed in calculating the $U(1)_X$ SSM. We show them in the appendix.

Here, we present some couplings required in this model

$$\mathcal{L}_{\tilde{\chi}^+ d \tilde{u}^*} = \sum_{a=1}^3 \tilde{\chi}_i^+ \left((-g_2 V_{i1}^* Z_{ka}^U + V_{i2}^* Y_{u,a} Z_{k3+a}^U) P_L + (Y_{d,a}^* Z_{ka}^U U_{i2}) P_R \right) d_{j\beta} \tilde{u}_{k\gamma}^* C_{ja}, \quad (27)$$

$$\mathcal{L}_{\tilde{\chi}^0 d \tilde{d}^*} = -\frac{1}{6} \tilde{\chi}_i^0 \left\{ (\sqrt{2} g_1 N_{i1}^* Z_{ka}^D - 3\sqrt{2} g_2 N_{i2}^* Z_{ka}^D + \sqrt{2} g_{YX} N_{i5}^* Z_{ka}^D + 6N_{i3}^* Y_{d,a} Z_{k3+a}^D) P_L + \right. \\ \left. (6Y_{d,a}^* Z_{kb}^D N_{i3} + \sqrt{2} Z_{k3+a}^D [2g_1 N_{i1} + (2g_{YX} + 3g_X) N_{i5}]) P_R \right\} d_{j\beta} \tilde{d}_{k\gamma}^*, \quad (28)$$

$$\mathcal{L}_{h H^- W^+} = \frac{1}{2} g_2 h_i \left(Z_{i1}^H Z_{j1}^- - Z_{i2}^H Z_{j2}^- \right) \left(-p_\mu^{H_j^-} + p_\mu^{h_i} \right) H_j^- W_\mu^+, \quad (29)$$

$$\mathcal{L}_{h W^+ W^-} = \frac{1}{2} g_2^2 h_i \left(v_d Z_{i1}^H + v_u Z_{i2}^H \right) g_{\sigma\mu} W_\sigma^+ W_\mu^-. \quad (30)$$

Here $P_L = \frac{1-\gamma^5}{2}$, $P_R = \frac{1+\gamma^5}{2}$, N , Z^D and Z^U , are the diagonalizing matrices for $M_{\tilde{\chi}^0}$, M_D^2 and M_U^2 . They satisfy the relations $N^T M_{\tilde{\chi}^0} N = \text{diag}(m_{\tilde{\chi}_1^0}, m_{\tilde{\chi}_2^0}, \dots, m_{\tilde{\chi}_8^0})$ and $Z_{\tilde{D}(\tilde{U})}^\dagger M_{\tilde{D}(\tilde{U})}^2 Z_{\tilde{D}(\tilde{U})} =$

$diag(m_{\tilde{D}(\tilde{U})_1}^2, m_{\tilde{D}(\tilde{U})_2}^2, \dots, m_{\tilde{D}(\tilde{U})_6}^2)$, where $m_{\tilde{\chi}_i^0}$ ($i = 1, 2, \dots, 8$) and $m_{\tilde{D}(\tilde{U})_i}^2$ ($i = 1, 2, \dots, 6$) denote the corresponding mass eigenvalues of $M_{\tilde{\chi}^0}$ and $M_{\tilde{D}(\tilde{U})}^2$.

There is a necessity for additional vertices, and in order to maintain brevity within the text, the remaining vertices can be accessed in Refs.[24, 26, 27].

III. PROCESS ANALYSIS

In this section, we investigate the amplitude and branching ratio of $h \rightarrow bs$. The corresponding Feynman diagrams are depicted in Fig.1. For example, we analyze one of the Feynman diagrams in Fig.1. The Feynman amplitude of Fig.1(a) is

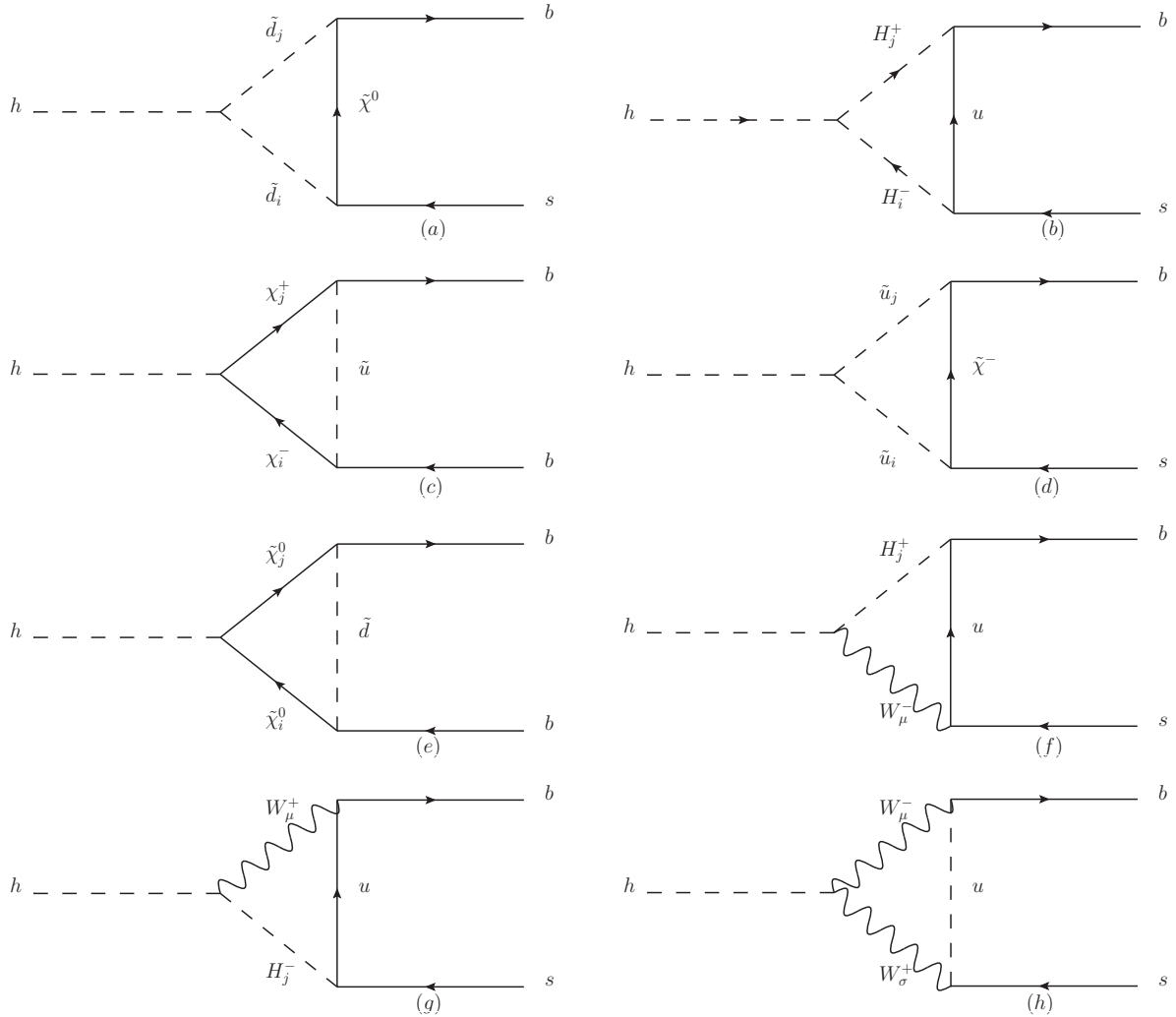


FIG. 1: Feynman diagrams for the $h \rightarrow bs$ process in the $U(1)_X$ SSM.

$$\mathcal{M}_{(a)} = \bar{U}_b(p) \int \frac{d^D k}{(2\pi)^D} \frac{1}{[(k+q)^2 - m_{\chi_0^2}^2][(p+q+k)^2 - m_{\tilde{d}_j}^2]} \frac{1}{(k^2 - m_{\tilde{d}_i}^2)} \left((B_L P_L + B_R P_R)(\not{k} + \not{q} - m_{\chi^0})(A_L P_L + A_R P_R) \right) C_1 U_s(q). \quad (31)$$

In this expression, p represents the momentum of the bottom quark (b), q corresponds to the momentum of the strange quark (s), and k is the loop momentum. The $m_{\tilde{d}_{i(j)}}$ term corresponds to the mass of the down–squark. $A_L, B_L, A_R,$ and B_R represent the coupling vertices mentioned in Section II. $\bar{U}_{b(p)}$ and $U_{s(q)}$ represent the wave functions of the bottom and strange quarks. C_1 is the coupling constant of $h\tilde{d}_i\tilde{d}_j$. The subscripts L and R represent the left–handed and right–handed parts, respectively.

In the subsequent calculations, we initially address the resolution of the Feynman integral, utilizing the formula specified in Ref.[31] for the integration of the denominator

$$\frac{1}{ABC} = \int_0^1 dx \int_0^1 2ydy \frac{1}{[(Ax + B(1-x))y + C(1-y)]^3}. \quad (32)$$

Performing the integral calculation in this manner can significantly enhance the efficiency of numerical computations in our work. Based on Eq(32), we arrive at

$$\begin{aligned} & \int_0^1 dx \int_0^1 2ydy \left\{ \left([(k+q)^2 - m_{\chi_0^2}^2]x + (k^2 - m_{\tilde{D}_j}^2)(1-x) \right) y \right. \\ & \left. + (k^2 + p^2 + q^2 - m_{\tilde{D}_i}^2)(1-y) \right\}^{-3} \\ & = \int_0^1 dx \int_0^1 2ydy \frac{1}{(k'^2 - J)^3}. \end{aligned} \quad (33)$$

Here, we let $(p+q)xy + q(1-y) = T, k+T = k'$ and $J = -p^2xy + q^2[xy + (1-y)]^2 + 2p \cdot q[xy(xy-y)] + xy + (1-y) + m_{\chi_0^2}^2(1-y) + m_{\tilde{d}_i}^2xy + m_{\tilde{d}_j}^2(1-y)y$ to obtain the final form of the denominator in Eq(31).

Subsequently, we utilize D–dimensional spatial integration to perform relevant calculations on the denominators

$$\int \frac{d^D k'}{(2\pi)^D} \frac{(k^2)^\alpha}{(k^2 - R^2)^\beta} = i \frac{(-1)^{\alpha-\beta} \Gamma(1 + \frac{D}{2}) \Gamma(\beta - \alpha - \frac{D}{2})}{(4\pi)^{\frac{D}{2}} \Gamma(\frac{D}{2}) \Gamma(\beta) (R^2)^{\beta - \alpha - \frac{D}{2}}}, \quad (34)$$

We use dimensional regularization to handle divergent terms, where $d = 4 - 2\epsilon$ and take the limit as d approaches 4. To obtain finite results, the divergent terms are canceled out by the modified minimal subtraction (\overline{MS}) scheme.

The final integral result we get is

$$\begin{aligned} \mathcal{M}_{(a)} = & \int_0^1 dx \int_0^1 2ydy \left(\frac{-A_L B_L m_{\chi^0} - A_L B_R m_b xy - A_L B_R m_s xy + A_L B_R m_s y}{64\pi^2 J} \right) C_1 \gamma^5 \\ & + \frac{m_b A_L B_R C_1 xy}{64\pi^2 J} + m_s C_1 \frac{A_L B_R xy - A_L B_R y}{64\pi^2 J} + \frac{m_{\chi^0} A_L B_L C_1}{64\pi^2 J} + (L \rightarrow R). \end{aligned} \quad (35)$$

We process all the diagrams in Fig.1 according to the aforementioned methods and further simplify them.

Due to the immense complexity of the calculations involved, we employ *Mathematica* \ll *HighEnergyPhysics'FeynCalc'* package for analytical computations. We derive the Feynman amplitudes for all the diagrams, and use the on-shell condition for the external particles $p^2 = m_b^2$, $q^2 = m_s^2$, $(p+q)^2 = m_h^2$. Subsequently, we perform summation operations and compute the squared modulus of the amplitudes, denoted as $|\mathcal{M}|^2$.

Ultimately, the decay width Γ of $h \rightarrow bs$ is obtained by substituting $|\mathcal{M}|^2$ into the following formula[8]

$$\Gamma(h \rightarrow bs) = 2N_c \frac{\lambda^{\frac{1}{2}}(m_h^2, m_b^2, m_s^2)}{16\pi m_h^3} |\mathcal{M}|^2, \quad (36)$$

here, $N_c = 3$ is a color factor, $\lambda(x, y, z) = (x - y - z)^2 - 4y^2 z^2$.

The branching ratio we obtained is

$$Br(h \rightarrow bs) = \frac{\Gamma(h \rightarrow bs)}{\Gamma(h)}. \quad (37)$$

here, $\Gamma(h) = 3.2 \times 10^{-3} \text{GeV}$ [32].

IV. NUMERICAL ANALYSIS

In analyzing the numerical values, we consider the experimental constraints to study the flavor-changing neutral current process $h \rightarrow bs$, subject to the following restrictions

1. The mass of the lightest CP-even Higgs, designated as m_h , approximately equals 125.25 GeV[32]. Due to the disruption of the orbit, our result of $Br(h \rightarrow bs)$ must fall within the 3σ range of the Higgs boson mass. Currently, the mass of the Higgs boson, with 3σ level errors, is obtained

$$m_h = 125.25 \pm 0.51 \text{GeV}. \quad (38)$$

2. The Higgs h decays($h \rightarrow \gamma + \gamma, Z + Z, W + W, b + \bar{b}, \tau + \bar{\tau}$)[29] should be satisfied.

3. Muon anomalous magnetic dipole moment is also taken into account[33, 34].

4. The mass of the chargino should exceed 1000 GeV, while the masses of up–squarks and down–squarks should be greater than 1400 GeV, and the mass of the slepton should be more than 600 GeV.

In the calculations, we take the up quark mass $m_u = 0.0022$ GeV, the down quark mass $m_d = 0.0047$ GeV, the strange quark mass $m_s = 0.095$ GeV, the bottom quark mass $m_b = 4.18$ GeV, the charm quark mass $m_c = 1.275$ GeV, the top quark mass $m_t = 173.5$ GeV, the W boson mass $m_W = 80.385$ GeV, the Z boson mass $m_Z = 91.188$ GeV, the electron mass $m_e = 0.500$ GeV, the muon mass $m_\mu = 0.105$ GeV, $\alpha(m_Z) = 1/128$, $\alpha_s(m_Z) = 0.118$.

We use images to visualize the effects of variables on the results, where the quantitative parameters are set as follows

$$\begin{aligned} \mu = 0.8\text{TeV}, \quad M_S = 3.6\text{TeV}, \quad v_S = 4.3\text{TeV}, \quad \kappa = 0.1, \quad \lambda_C = -0.08, \\ M_{\tilde{q}11}^2 = M_{\tilde{q}22}^2 = 1.9^2\text{TeV}^2, \quad M_{\tilde{u}11}^2 = M_{\tilde{u}22}^2 = 1.9^2\text{TeV}^2, \quad M_{\tilde{q}33}^2 = M_{\tilde{u}33}^2 = 6\text{TeV}^2. \end{aligned} \quad (39)$$

To streamline the numerical investigation, we use the interdependency of the parameters, which undergo variations throughout the subsequent numerical analysis

$$\begin{aligned} g_X, \quad g_{YX}, \quad \tan\beta, \quad \lambda_H, \quad M_1, \quad M_2, \\ M_{BL}, \quad M_{BB'}, \quad M_{dij}^2 = M_{dji}^2, \quad (i, j = 1, 2, 3, i \neq j). \end{aligned} \quad (40)$$

Typically, the non-diagonal elements of the parameters are set to zero as a default, unless explicitly stated otherwise.

A. one-dimensional line graph

In this subsection, we conduct numerical calculations for $\text{Br}(h \rightarrow bs)$ and plot correlation graphs for various parameters to clearly illustrate the numerical results. We use the parameters as $\tan\beta = 13$, $M_1 = 0.7$ TeV, $M_2 = 1.2$ TeV, $(M_d)_{11}^2 = (M_d)_{22}^2 = (M_d)_{33}^2 = 2.70$ TeV^2 , $M_{BL} = 0.7$ TeV, $M_{BB'} = 0.4$ TeV. In the context of $U(1)_X$ SSM, g_{YX} is the mixing gauge coupling constant, which affects the strength of the coupling vertices. To investigate its impact on the $\text{Br}(h \rightarrow bs)$, we vary g_{YX} within the range of (0.1–0.24). Additionally, considering g_X and λ_H as two sensitive parameters, we adjust g_X within (0.24–0.48) and

λ_H within (0.08–0.20). Through data analysing, we plot the relationships between g_{YX} and $\text{Br}(h \rightarrow bs)$, g_X and $\text{Br}(h \rightarrow bs)$, as well as λ_H and $\text{Br}(h \rightarrow bs)$ in Fig.2.

Fig.2(a) and Fig.2(b) illustrate the correlation between g_X , g_{YX} , and $\text{Br}(h \rightarrow bs)$, where we compare the values by varying g_{YX} and g_X . We observe that, within the g_X range of 0.24 to 0.48, the corresponding values of the lines gradually increase with the increase of g_X , and the values also increase when g_{YX} is increased. Similarly, in the g_{YX} range of 0.10 to 0.23, the corresponding values of the lines gradually increase with the increase of g_{YX} , and the values also increase when g_X is increased. Fig.2(c) represents the relationship between λ_H and $\text{Br}(h \rightarrow bs)$. Within the λ_H range of 0.08 to 0.19, the corresponding values of the lines decrease as λ_H increases. Yet, they also increase when the value of g_{YX} is incremented. Notably, the value of $\text{Br}(h \rightarrow bs)$ falls within the range of $(1 \sim 5) \times 10^{-3}$.

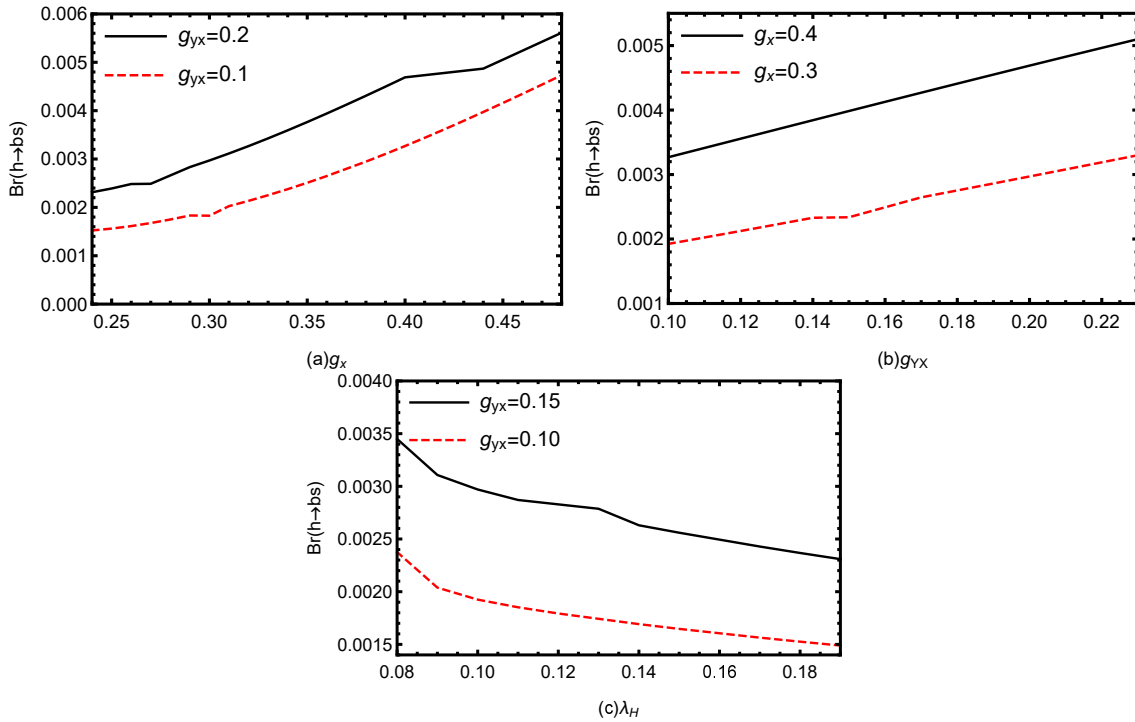


FIG. 2: The influence of various parameters on $\text{Br}(h \rightarrow bs)$: In (a) and (b), $\lambda_H = 0.1$, and in (c), $g_X = 0.3$.

B. two-dimensional scatter plot

To better study the influence of parameters, we draw some multidimensional scatter plots based on χ^2 and select values that fall within 3σ range of χ^2 , ensuring a more significant correlation between the variables and $\text{Br}(h \rightarrow bs)$. We utilize the simplified expression of χ^2 as

$$\chi^2 = \sum_i \left(\frac{\mu_i^{th} - \mu_i^{exp}}{\delta_i} \right)^2. \quad (41)$$

In Eq.(41), μ_i^{th} signifies the theoretical value for the corresponding procedure derived within $U(1)_X\text{SSM}$. The experimental data is denoted as μ_i^{exp} , while δ_i represents the error encompassing both statistical and systematic components.

The specific expression of χ^2 is presented as

$$\begin{aligned} \chi^2 = & \left(\frac{m_{h^0}^{th} - m_{h^0}^{exp}}{\delta_{m_{h^0}}} \right)^2 + \left(\frac{\mu_{\gamma\gamma}^{th} - \mu_{\gamma\gamma}^{exp}}{\delta_{\gamma\gamma}} \right)^2 + \left(\frac{\mu_{ZZ}^{th} - \mu_{ZZ}^{exp}}{\delta_{ZZ}} \right)^2 \\ & + \left(\frac{\mu_{WW}^{th} - \mu_{WW}^{exp}}{\delta_{WW}} \right)^2 + \left(\frac{\mu_{bb}^{th} - \mu_{bb}^{exp}}{\delta_{bb}} \right)^2 + \left(\frac{\mu_{\tau\bar{\tau}}^{th} - \mu_{\tau\bar{\tau}}^{exp}}{\delta_{\tau\bar{\tau}}} \right)^2 + \left(\frac{\Delta a_\mu^{th} - \Delta a_\mu}{\delta_{\Delta a_\mu}} \right)^2. \end{aligned} \quad (42)$$

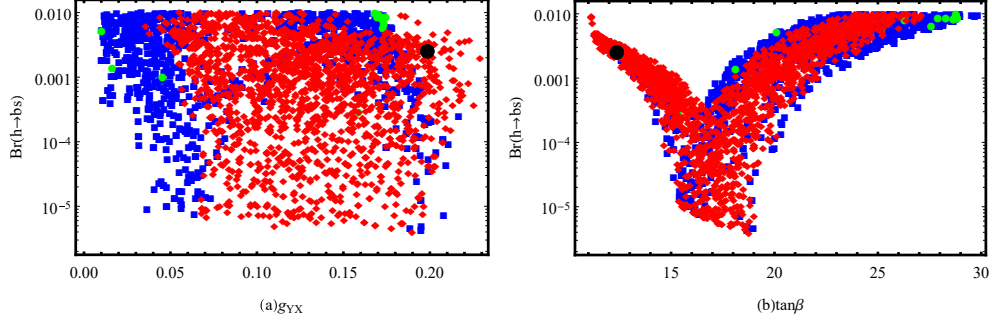
The averaged values of the experimental data are derived from the updated PDG [20], $m_{h^0}^{exp} = 125.25 \pm 0.17$ GeV, $\mu_{\gamma\gamma}^{exp} = 1.10 \pm 0.07$, $\mu_{ZZ}^{exp} = 1.01 \pm 0.07$, $\mu_{WW}^{exp} = 1.19 \pm 0.12$, $\mu_{bb}^{exp} = 0.98 \pm 0.12$, $\mu_{\tau\bar{\tau}}^{exp} = 1.15 \pm 0.15$. $\Delta a_\mu = (2.50 \pm 0.48) \times 10^{-9}$ is obtained from the latest work of muon g-2 [30-31].

We plot the relationship between parameters based on three σ ranges of χ^2 , and they are presented in Fig.3 , Fig.4 and Fig.5. The black circle denotes optimally fitted benchmark point with a χ^2 value of 5.11 ($\chi_{min}^2 = 5.11$). The red-shaded region signifies a confidence level of 68.3%, encompassing values of χ^2 that are within or equal to $\chi_{min}^2 + 9.3$. The blue area highlights a confidence level of 95.45%, corresponding to χ^2 values that exceed $\chi_{min}^2 + 9.3$ but remain below $\chi_{min}^2 + 15.78$. Lastly, the green-colored section represents the 99.73% confidence interval, spanning the range from $\chi_{min}^2 + 15.78$ to $\chi_{min}^2 + 23.54$.

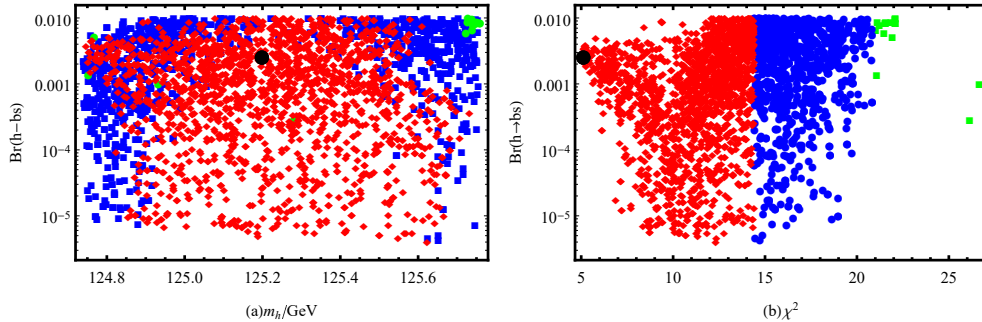
Subsequently, we randomly scan eight parameters and present them in Table II. Fig.3 , Fig.4 and Fig.5 are plotted using the parameters present in Table II. \blacklozenge is a value located within the 1σ range of χ^2 in the domain of $\chi^2 \leq 14.41$. \blacksquare is a value situated within the 2σ range of χ^2 , where $14.41 \leq \chi^2 \leq 20.89$. \bullet is a value situated within the 3σ range of χ^2 , where again $20.89 \leq \chi^2 \leq 28.65$. \bullet represents the value corresponding to the optimal point.

TABLE II: Scanning parameters for Fig.3 Fig.4 and Fig.5.

Parameters	g_X	g_{YX}	$\tan \beta$	M_1/ TeV	M_2/ TeV	M_{BL}/ TeV	$M_{BB'}/ \text{TeV}$	M_d^2/ TeV^2
Min	0.3	0.01	8	0.2	1	0.1	0.1	4
Max	0.4	0.3	35	1	2	1	1	16


 FIG. 3: The χ^2 plot in the $g_{YX}-\text{Br}(h \rightarrow bs)$ plane; The χ^2 plot in the $\tan \beta-\text{Br}(h \rightarrow bs)$ plane.

From eight parameters, we select two sensitive parameters g_{YX} and $\tan \beta$ to show the results, and plot the graphs respectively using g_{YX} and $\tan \beta$ as the horizontal axes and $\text{Br}(h \rightarrow bs)$ as the vertical axis in Fig.3. These two parameters exhibit significant influence on $\text{Br}(h \rightarrow bs)$. As seen in Fig.3(a), most of the points are distributed within the range of $0.05 \leq g_{YX} \leq 0.20$ and $10^{-4} \leq \text{Br}(h \rightarrow bs) \leq 10^{-2}$. When $g_{YX} \geq 0.2$ and $\text{Br}(h \rightarrow bs) \leq 10^{-4}$, the density of points gradually decreases. In Fig.3(b), the majority of points are situated within the range of $11 \leq \tan \beta \leq 29$ and $5 \times 10^{-4} \leq \text{Br}(h \rightarrow bs) \leq 0.01$. When $15 \leq \tan \beta \leq 20$ and $\text{Br}(h \rightarrow bs) \leq 5 \times 10^{-4}$, the distribution of points becomes less dense. By combining the insights from Fig.3(a) and Fig.3(b), it is evident that when $g_{YX} \approx 0.20$ and $\tan \beta \approx 12$, χ^2 reaches its optimal value, resulting in $\text{Br}(h \rightarrow bs)$ of 2.5×10^{-3} .


 FIG. 4: The χ^2 plot in the $m_h-\text{Br}(h \rightarrow bs)$ plane; The χ^2 plot in the $\chi^2-\text{Br}(h \rightarrow bs)$ plane.

Here, in Fig.4(a), we present a scatter plot of m_h with $\text{Br}(h \rightarrow bs)$. It can be observed that the optimal point of χ^2 is located near $m_h = 125.2$ GeV, which aligns well with the mass of the CP-even Higgs. As the mass of m_h increases or decreases from 125.2 GeV within the 3σ range, the density of points gradually enhances, and the points also cluster around the $\text{Br}(h \rightarrow bs)$ of the order of 10^{-3} . Fig.4(b) depicts a scatter plot of χ^2 with $\text{Br}(h \rightarrow bs)$, clearly illustrating the distribution of $\text{Br}(h \rightarrow bs)$ as χ^2 varies.

C. the Significant Impact of a_μ on Numerical Calculations

Next, we investigate the relation of muon magnetic dipole moment (MDM) with the flavor violation of $h \rightarrow bs$. The E989 collaboration at Fermilab [35] report the latest experimental data as $a_\mu^{FNAL} = 116592055(24) \times 10^{-11}$. The new averaged experiment value of muon MDM is $a_\mu^{exp} = 116592059(22) \times 10^{-11}$. Therefore, there is a deviation of 5.0σ between the experiment and SM expectation ($\Delta a_\mu = a_\mu^{exp} - a_\mu^{SM} = 249(48) \times 10^{-11}$)[36].

In Fig.5, we present a series of scatter plots to illustrate the correlations between $\tan \beta$, m_h , g_{YX} , $\text{Br}(h \rightarrow bs)$, χ^2 , and a_μ . The vertical axis of Fig.5(a) is g_{YX} , the vertical axis of Fig.5(b) is $\tan \beta$, the vertical axis of Fig.5(c) is m_h , the vertical axis of Fig.5(d) is $\text{Br}(h \rightarrow bs)$, and the vertical axis of Fig.5(e) is χ^2 . To clarify, the blue portion represents the $1\sigma(2.02 \times 10^{-9} \leq a_\mu \leq 2.50 \times 10^{-9})$ range of a_μ , the pink portion represents the $2\sigma(1.54 \times 10^{-9} \leq a_\mu \leq 2.02 \times 10^{-9})$ range, and the yellow portion represents the $3\sigma(1.06 \times 10^{-9} \leq a_\mu \leq 1.54 \times 10^{-9})$ range. Due to the limited number of data points, we will focus our analysis on the first half of the experimental limitations. We can easily observe that the numerical results of χ^2 are all within the 3σ experimental limit of a_μ , and the χ^2 optimal point located at the $1\sigma(2.02 \times 10^{-9} \leq a_\mu \leq 2.50 \times 10^{-9})$ position of a_μ . These indicate that with the optimal value of χ^2 , the numerical results of a_μ can effectively compensate for the deviation between the experimental values and the SM predicted values. The parameters $\tan \beta$, m_h , and g_{YX} are still significant factors that have a considerable impact on $\text{Br}(h \rightarrow bs)$. Compared with the previous section, after adding restrictions of a_μ , we obtain more precise parameter spaces.

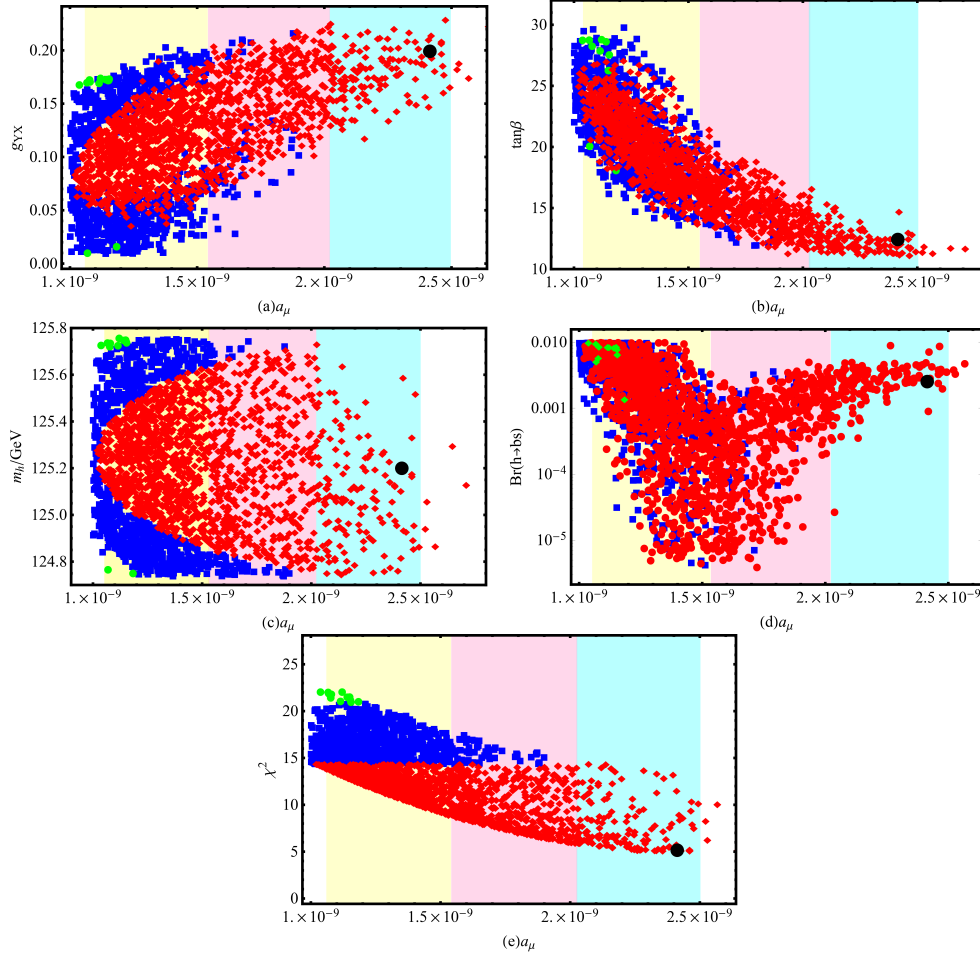


FIG. 5: The relation of a_μ with other parameters

V. CONCLUSION

In the $U(1)_X$ SSM, we analyze the phenomenology of flavor-changing decays of the Higgs boson to a strange-bottom quark pair. We assume that the lightest CP-even Higgs boson, denoted as h , is the SM-like Higgs boson discovered by the LHC. A significant focus of this paper is to analyze the $U(1)_X$ SSM contributions with h .

From the perspective of the magnitude of $\text{Br}(h \rightarrow bs)$ and data analysis, the $\text{Br}(h \rightarrow bs)$ can reach the order of 10^{-3} , which is four orders of magnitude larger compared with the prediction SM. Experimental values are more precise. We consider the Feynman diagrams for the $h \rightarrow bs$ process and perform extensive calculations, plotting linear graphs of various parameters versus $\text{Br}(h \rightarrow bs)$. To enhance the fitting degree of the numerical analysis, we include χ^2 and conduct a broad scan of the parameters. Through numerical analysis, we

find that a subset of parameters exert a significant influence on the results. M_1 , M_2 , M_{BL} , $M_{BB'}$, and M_d^2 are the unsensitive parameters, while g_X , g_{YX} , $\tan \beta$, and λ_H are the sensitive parameters. Finally, we analyze the relationship between a_μ and other sensitive parameters, as well as the correlation between a_μ and $\text{Br}(h \rightarrow bs)$. Through comprehensive research, we have demonstrated that all parameters in our work satisfy the constraints from $h \rightarrow bs$ process. However, such decays remain undetectable at the LHC[37, 38]. We believe that our findings may serve as a valuable resource for those interesting decays within alternative frameworks of new physics.

Acknowledgments

This work is supported by National Natural Science Foundation of China (NNSFC)(No.12075074), Natural Science Foundation of Hebei Province(A2020201002, A2023201040, A2022201022, A2022201017, A2023201041), Natural Science Foundation of Hebei Education Department (QN2022173), Post-graduate's Innovation Fund Project of Hebei University (HBU2024SS042), the youth top-notch talent support program of the Hebei Province.

Appendix A: Used mass matrices in $U(1)_X$ SSM

The mass squared matrix for Up-Squarks ($\tilde{u}_L^0, \tilde{u}_R^0$) reads

$$M_{\tilde{U}}^2 = \begin{pmatrix} m_{\tilde{u}_L^0 \tilde{u}_L^{0,*}} & m_{\tilde{u}_R^0 \tilde{u}_L^{0,*}}^\dagger \\ m_{\tilde{u}_L^0 \tilde{u}_R^{0,*}} & m_{\tilde{u}_R^0 \tilde{u}_R^{0,*}} \end{pmatrix}, \quad (\text{A1})$$

$$m_{\tilde{u}_L^0 \tilde{u}_L^{0,*}} = \frac{1}{24} \left(3g_2^2(-v_u^2 + v_d^2) + (g_1^2 + g_{YX}^2)(-v_d^2 + v_u^2) + g_{YX}g_X(2v_\eta^2 - 2v_\eta^2 - v_d^2 + v_u^2) \right) + \frac{1}{2}(2m_{\tilde{Q}}^2 + v_u^2 Y_u^\dagger Y_u), \quad (\text{A2})$$

$$m_{\tilde{u}_L^0 \tilde{u}_R^{0,*}} = -\frac{1}{2} \left(\sqrt{2}(v_d Y_u \mu^* - v_u T_u) + v_d v_s Y_u \lambda_H^* \right), \quad (\text{A3})$$

$$m_{\tilde{u}_R^0 \tilde{u}_R^{0,*}} = \frac{1}{24} \left(4(g_1^2 + g_{YX}^2)(-v_u^2 + v_d^2) + g_{YX}g_X(7v_d^2 - 7v_u^2 - 8v_\eta^2 + 8v_\eta^2) \right) + 3g_X^2(-2v_\eta^2 + 2v_\eta^2 - v_u^2 + v_d^2) + \frac{1}{2}(2m_{\tilde{U}}^2 + v_u^2 Y_u Y_u^\dagger). \quad (\text{A4})$$

The mass squared matrix for Down-Squarks ($\tilde{d}_L^0, \tilde{d}_R^0$) reads

$$M_D^2 = \begin{pmatrix} m_{\tilde{d}_L^0 \tilde{d}_L^{0,*}} & m_{\tilde{d}_R^0 \tilde{d}_L^{0,*}}^\dagger \\ m_{\tilde{d}_L^0 \tilde{d}_R^0} & m_{\tilde{d}_R^0 \tilde{d}_R^{0,*}} \end{pmatrix}, \quad (\text{A5})$$

$$m_{\tilde{d}_L^0 \tilde{d}_L^{0,*}} = \frac{1}{24} \left((3g_2^2 + g_1^2 + g_{YX}^2)(-v_d^2 + v_u^2) + g_{YX}g_X(2v_\eta^2 - 2v_\eta^2 - v_d^2 + v_u^2) \right) + \frac{1}{2}(2m_Q^2 + v_d^2 Y_d^\dagger Y_d), \quad (\text{A6})$$

$$m_{\tilde{d}_L^0 \tilde{d}_R^0} = -\frac{1}{2} \left(\sqrt{2}(-v_d T_d + v_u Y_d \mu^*) + v_u v_s Y_d \lambda_H^* \right), \quad (\text{A7})$$

$$m_{\tilde{d}_R^0 \tilde{d}_R^{0,*}} = \frac{1}{24} \left(2(g_1^2 + g_{YX}^2)(-v_u^2 + v_d^2) + g_{YX}g_X(-4v_\eta^2 + 4v_\eta^2 + 5v_d^2 - 5v_u^2) \right) + 3g_X^2(-2v_\eta^2 + 2v_\eta^2 - v_u^2 + v_d^2) + \frac{1}{2}(2m_D^2 + v_d^2 Y_d Y_d^\dagger). \quad (\text{A8})$$

The mass matrix for neutralino in the basis $(\lambda_{\tilde{B}}, \tilde{W}^0, \tilde{H}_d^0, \tilde{H}_u^0, \lambda_{\tilde{X}}, \tilde{\eta}, \tilde{\eta}, \tilde{s})$ is

$$M_{\tilde{\chi}^0} = \begin{pmatrix} M_1 & 0 & -\frac{g_1}{2}v_d & \frac{g_1}{2}v_u & M_{BB'} & 0 & 0 & 0 \\ 0 & M_2 & \frac{g_2}{2}v_d & -\frac{g_2}{2}v_u & 0 & 0 & 0 & 0 \\ -\frac{g_1}{2}v_d & \frac{g_2}{2}v_d & 0 & m_{\tilde{H}_d^0 \tilde{H}_d^0} & m_{\lambda_{\tilde{X}} \tilde{H}_d^0} & 0 & 0 & -\frac{\lambda_H v_u}{\sqrt{2}} \\ \frac{g_1}{2}v_u & -\frac{g_2}{2}v_u & m_{\tilde{H}_d^0 \tilde{H}_u^0} & 0 & m_{\lambda_{\tilde{X}} \tilde{H}_u^0} & 0 & 0 & -\frac{\lambda_H v_d}{\sqrt{2}} \\ M_{BB'} & 0 & m_{\tilde{H}_d^0 \lambda_{\tilde{X}}} & m_{\tilde{H}_u^0 \lambda_{\tilde{X}}} & M_{BL} & -g_X v_\eta & g_X v_{\tilde{\eta}} & 0 \\ 0 & 0 & 0 & 0 & -g_X v_\eta & 0 & \frac{1}{\sqrt{2}}\lambda_C v_S & \frac{1}{\sqrt{2}}\lambda_C v_{\tilde{\eta}} \\ 0 & 0 & 0 & 0 & g_X v_{\tilde{\eta}} & \frac{1}{\sqrt{2}}\lambda_C v_S & 0 & \frac{1}{\sqrt{2}}\lambda_C v_\eta \\ 0 & 0 & -\frac{1}{\sqrt{2}}\lambda_H v_u & -\frac{1}{\sqrt{2}}\lambda_H v_d & 0 & \frac{1}{\sqrt{2}}\lambda_C v_{\tilde{\eta}} & \frac{1}{\sqrt{2}}\lambda_C v_\eta & m_{\tilde{s}\tilde{s}} \end{pmatrix}, \quad (\text{A9})$$

$$m_{\tilde{H}_d^0 \tilde{H}_u^0} = -\frac{1}{\sqrt{2}}\lambda_H v_S - \mu, \quad m_{\tilde{H}_d^0 \lambda_{\tilde{X}}} = -\frac{1}{2}(g_{YX} + g_X)v_d, \\ m_{\tilde{H}_u^0 \lambda_{\tilde{X}}} = \frac{1}{2}(g_{YX} + g_X)v_u, \quad m_{\tilde{s}\tilde{s}} = 2M_s + \sqrt{2}\kappa v_S. \quad (\text{A10})$$

The mass matrix for charged Higgs in the basis: $(H_d^-, H_u^{+,*}), (H_d^{-,*}, H_u^+)$

$$M_{H^\pm} = \begin{pmatrix} m_{H_d^- H_d^{-,*}} & m_{H_u^{+,*} H_d^{-,*}}^* \\ m_{H_d^- H_u^+} & m_{H_u^{+,*} H_u^+} \end{pmatrix}, \quad (\text{A11})$$

$$m_{H_d^- H_d^{-,*}} = \frac{1}{8} \left((g_2^2 + g_X^2)v_d^2 + (g_2^2 - g_X^2)v_u^2 + (g_1^2 + g_{YX}^2)(v_d^2 - v_u^2) - 2g_X^2 v_\eta^2 \right) + 2[g_{YX}g_X(v_d^2 + v_\eta^2 - v_\eta^2 - v_u^2) + g_X^2 v_\eta^2]$$

$$+ \left(|\mu|^2 + \sqrt{2}v_S \Re(\mu\lambda_H^*) + \frac{1}{2}v_S^2 |\lambda_H|^2 \right), \quad (\text{A12})$$

$$m_{H_d^- H_u^+} = \frac{1}{2} \left(2(\lambda_H l_W^* + B_\mu) + \lambda_H (2\sqrt{2}v_S M_S^* - v_d v_u \lambda_H^* + v_\eta v_{\bar{\eta}} \lambda_C^* + \sqrt{2}v_S T_{\lambda_H}) \right) + \frac{1}{4} g_2^2 v_d v_u, \quad (\text{A13})$$

$$m_{H_u^{+,*} H_u^+} = \frac{1}{8} \left((g_2^2 - g_X^2) v_d^2 + (g_2^2 + g_X^2) v_u^2 + (g_1^2 + g_{YX}^2) (v_u^2 - v_d^2) - 2g_X^2 v_\eta^2 + 2[g_{YX} g_X (v_u^2 + v_\eta^2 - v_d^2 - v_\eta^2) + g_X^2 v_\eta^2] \right) + \frac{1}{2} \left(2|\mu|^2 + 2\sqrt{2}v_S \Re(\mu\lambda_H^*) + v_S^2 |\lambda_H|^2 \right). \quad (\text{A14})$$

- [1] ATLAS Publications, Phys. Lett. B **716** (2022) 1-29. [arXiv: 1207.7214].
- [2] CMS Collaboration, Phys. Lett. B **716** (2012) 30-61. [arXiv: 1207.7235].
- [3] J. Ren, et al., JHEP **06** (2018) 090. [arXiv: 1706.05980].
- [4] H. Sun, and Y.J. Zhou, JHEP **11** (2012) 127. [arXiv: 1211.6201].
- [5] M. Ibe, S. Matsumoto, and T.T. Yanagida, Phys. Rev. D **85** (2012) 095011. [arXiv: 1202.2253].
- [6] J.L. Evans, et al., Phys. Rev. D **85** (2012) 095004. [arXiv: 1201.2611].
- [7] M. Takeo and N. Kazunori, Phys. Lett. B **710** (2012) 159-163. [arXiv: 1112.3123].
- [8] F. Arco, S. Heinemeyer and M. J. Herrero, (2023). [arXiv: 2306.07958].
- [9] R. S. Willey, H. L. Yu, Phys. Rev. D **26** (1982) 3086-3091.
- [10] L G Benitez-Guzmán, et al., J. Phys. G **42** (2015) 085002. [arXiv: 1506.02718].
- [11] J I Aranda, et al., J. Phys. G **47** (2020) 125001. [arXiv: 2009.07166].
- [12] Gianluca Blankenburg, et al., Phys. Lett. B **712** (2012) 386-390. [arXiv: 1202.5704].
- [13] Barducci, Daniele and Helmboldt, et al., JHEP **12** (2017) 105. [arXiv: 1710.06657].
- [14] S.M. Zhao, T.F. Feng, and X.X. Dong, et al., Nucl. Phys. B **910** (2016) 225-239. [arXiv: 1603.09505].
- [15] S. Davidson and S. F. King, Phys. Lett. B **445** (1998) 191-198. [arXiv: 9808296].
- [16] C.X. Liu, H.B. Zhang, J.L. Yang, and S.M. Zhao, et al., JHEP **04** (2020) 002. [arXiv: 2002.04370].
- [17] H.B. Zhang and T.F. Feng, et al., JHEP **07** (2013) 069. [arXiv: 1305.4352].
- [18] G. Moulataka, et al., Eur. Phys. J. C **82** (2022) 657. [arXiv: 2202.06919].

- [19] S.M. Zhao, L.H. Su, X.X. Dong, et al., JHEP **03** (2022) 101.
- [20] B. Yan, S.M. Zhao and T.F. Feng, (2021). [arXiv: 2011.08533].
- [21] S.M. Zhao, T.F. Feng, M.J. Zhang, et al., JHEP **02** (2020) 130. [arXiv: 1905.11007].
- [22] M.Y. Liu, S.M. Zhao, S. Gao, L. Ruan, and T.F. Feng, (2024). [arXiv: 2405.00961].
- [23] Y.T. Wang, S.M. Zhao, et al., Phys. Rev. D **106** (2022) 055044. [arXiv: 2207.01770].
- [24] S.M. Zhao, G.Z.Ning, J.J. Feng, et al., Nucl. Phys. B **969** (2021) 115469.
- [25] A. Abdesslam, Phys. Lett. B **612** (2005) 263-274. [arXiv: 0409218].
- [26] S.M. Zhao, X. Wang, X.X. Dong, H.B. Zhang, and T.F. Feng, Symmetry **14** (2022) 2153. [arXiv: 2209.07094].
- [27] L.H. Su, S.M. Zhao, X.X. Dong, D.D. Cui, T.F. Feng and H.B. Zhang, Eur. Phys. J. C **81** (2021) 433 [arXiv: 2012.04824].
- [28] G. Bélanger, J. Da Silva and H.M. Tran, Phys. Rev. D **95** (2017) 115017 [arXiv: 1703.03275].
- [29] V. Barger, P. Fileviez Perez and S. Spinner, Phys. Rev. Lett. **102** (2009) 181802 [arXiv: 0812.3661].
- [30] P.H. Chankowski, S. Pokorski and J. Wagner, Eur. Phys. J. C **47** (2006) 187
- [31] B. L. Yang, Quantum Field Theory: From Operators to Path Integrals, World Scientific Publishing Co. (1988).
- [32] R. L. Workman, et al., (ParticleDataGroup), Prog.Theor.Exp.Phys. **2022** (2022) 083C01.
- [33] Á. S. de Jesus, F. S. Queiroz, J. W. F. Valle and Y. Villamizar, (2024). [arXiv: 2312.03851].
- [34] D. P. Aguillard et al., Phys. Rev. Lett. **131** (2023) 161802. [arXiv: 2308.06230].
- [35] D. P. Aguillard, et al. Phys. Rev. Lett. **131** (2023) 161802.
- [36] A. Datta, D. Marfatia and L. Mukherjee, Phys. Rev. D. **109** (2024) L031701.
- [37] G. Blankenburg, J. Ellis, and G. Isidori, Phys. Lett. B **712** (2012) 386.
- [38] R. Harnik, J. Kopp, and J. Zupan, JHEP **03** (2013) 026.